ACS central science

Research Article

Cite This: ACS Cent. Sci. 2019, 5, 1425−1431

http://pubs.acs.org/journal/acscii

Chemiresistive Sensing of Ambient CO_2 by an Autogenously Hydrated Cu_3(hexaiminobenzene)$_2$ Framework

Ivo Stassen,[†] Jin-Hu Dou,[†] Christopher Hendon,[⊥] and Mircea Dincă*[,†]

[†]Massachusetts Institute of Technology, Department of Chemistry, Cambridge, Massachusetts 02139, United States

[⊥]University of Oregon, Department of Chemistry and Biochemistry, Eugene, Oregon 97401, United States

Supporting Information

ABSTRACT: A growing demand for indoor atmosphere monitoring relies critically on the ability to reliably and quantitatively detect carbon dioxide. Widespread adoption of CO_2 sensors requires vastly improved materials and approaches because selective sensing of CO_2 under ambient conditions, where relative humidity (RH) and other atmosphere contaminants provide a complex scenario, is particularly challenging. This report describes an ambient CO_2 chemiresistor platform based on nanoporous, electrically conducting two-dimensional metal−organic frameworks (2D MOFs). The CO_2 chemiresistive sensitivity of 2D MOFs is attained through the incorporation of imino-semiquinonate moieties, i.e., well-defined N-heteroatom functionalization. The best performance is obtained with Cu_3(hexaiminobenzene)$_2$, Cu_3HIB_2, which shows selective and robust ambient CO_2 sensing properties at practically relevant levels (400−2500 ppm). The observed ambient CO_2 sensitivity is nearly RH-independent in the range 10−80% RH. Cu_3HIB_2 shows higher sensitivity over a broader RH range than any other known chemiresistor. Characterization of the CO_2-MOF interaction through a combination of in situ optical spectroscopy and density functional theory calculations evidence autogenously generated hydrated adsorption sites and a charge trapping mechanism as responsible for the intriguing CO_2 sensing properties of Cu_3HIB_2.

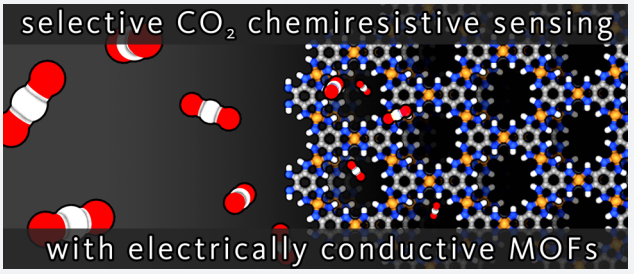

INTRODUCTION

Carbon dioxide shows vast potential as a gas-phase marker in natural, domestic, and industrial processes.[1,2] For example, using the indoor CO_2 level as a measure of human occupation can lead to smarter and more energy-efficient automation of buildings or vehicles.[3] Future Internet of things (IoT) devices able to perceive precise CO_2 levels may find use in health and safety applications such as surveillance,[4] food spoilage,[5] and air quality.[6]

Nondispersive infrared (NDIR) CO_2 optical sensors are well-established in a handful of practical applications.[7] However, even after decades of optimization, some inherent drawbacks of their optoelectronic mode of operation remain unresolved: device complexity, power consumption, scalability, and cost.[1,2] To enable the widespread adoption of CO_2 sensors in many aspects of modern society, inexpensive mass-producible devices are needed that offer simplicity, robustness, and ultralow power demand. Chemiresistors offer many of these benefits and are commercially already well-established in the form of metal oxide (MOx) sensors.[8] The operation principle of these simple, two-terminal passive components is based on conducting materials that transduce analyte−surface interactions to shifts in their current−voltage (I−V) characteristics. I−V curves correlate chemical states (e.g., target gas partial pressures) to the direct-current (DC) conductance, G, of a resistor (Figure 1a). However, in contrast to all combustible gases or vapors typically targeted by MOx sensors,[9] CO_2 detection by oxidative decomposition is not feasible because CO_2 cannot be further oxidized.

Analogous to the recent advances made for other classes of challenging analytes,[10] material developments on the molecular level are key to establishing practical CO_2 chemiresistors. Typical ambient CO_2 sensing applications would require quantitative sensing in 10−1000 ppm of CO_2 increments relative to the 0.04% (i.e., 400 ppm) atmospheric level, in air under a wide range of relative humidity (RH). Although many avenues of molecular and nanoscopic materials have been explored,[11,12] there are no materials that operate as efficient CO_2 chemiresistors within these boundary conditions. One popular means to enhance the CO_2 sensitivity and selectivity of chemiresistors is through functionalization with amine-rich nonconducting polymers, such as polyethylenimine (PEI),[13] which reversibly form acid−base adducts with CO_2 or catalyze the hydrolysis of CO_2 to carbonic acid and bicarbonates.[14−17] However, these composite amine-rich sensors display sharply decreasing sensitivity even for moderate drops in RH because dehydrated sensors gradually lose their ability to transduce interactions with CO_2.[15−19]

Electrically conducting two-dimensional metal−organic frameworks (2D MOFs) are an emergent class of nanoporous hybrid materials built from redox-active organic ligands and

Received: May 15, 2019
Published: June 27, 2019

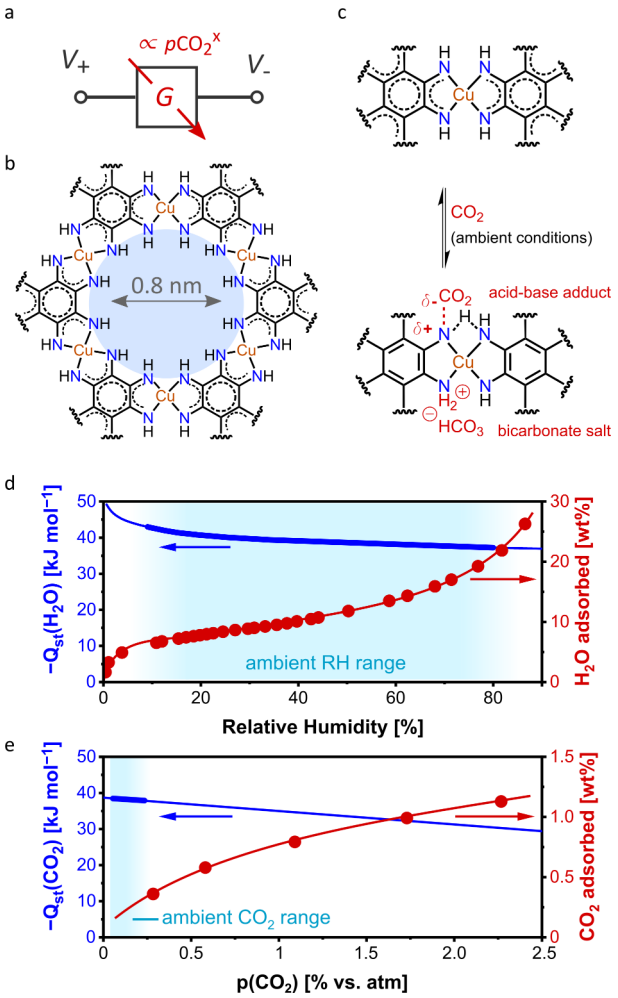

Figure 1. Conducting two-dimensional metal−organic framework (2D MOF) Cu_3HIB_2 for CO_2 sensing: (a) Representation of the target of this study: conductance modulation of a chemiresistor by the partial pressure of CO_2, pCO_2^x; (b) portion of the Cu_3HIB_2 honeycomb lattice, displaying the intrinsic cavity and the high density of accessible NH moieties; (c) proposed molecular interactions occurring at the organic−inorganic node of Cu_3HIB_2 exposed to ambient CO_2: formation of acid−base adducts and formation of bicarbonate salts by base-catalyzed hydrolysis; (d) isosteric heat of water adsorption and water adsorption isotherm for Cu_3HIB_2 at 20 °C; (e) isosteric heat of CO_2 adsorption and CO_2 adsorption isotherm for Cu_3HIB_2 at 20 °C.

transition metal inorganic nodes.[20−22] The unique combination of electrical conductivity and intrinsic nanoporosity raises the intriguing potential to use 2D MOFs as chemical sensors.[23,24] Their utility in this respect has already been demonstrated with redox-active gases or condensable vapors, but none of these prior studies have identified efficient materials for the particularly difficult CO_2 analyte, nor have they focused on addressing moisture as a significant interference.[25−30]

Herein, we propose a platform for ambient CO_2 sensing based on conducting 2D MOFs that are autogenously hydrated and comprise imino-semiquinonate (NH) moieties. As proof of concept, we demonstrate Cu_3(hexaiminobenzene)$_2$, Cu_3HIB_2, sensors prepared by simple drop-casting of as-synthesized polycrystalline material on interdigitated electrodes. Sensors made from Cu_3HIB_2 are capable of detecting small variations in the atmospheric CO_2 level. Their sensitivity in the 400−1000 ppm range, −0.62% (100 ppm)$^{-1}$, is remarkably invariant with relative humidity (RH) and is the highest among any other materials in the broad range 10−80% RH. In situ diffuse-reflectance spectroscopy (DRS) points toward analyte-induced charge trapping as the mechanism behind the observed response of the sensors.

RESULTS AND DISCUSSION

The recently reported Cu_3HIB_2 (Figure 1b)[31−33] combines favorable design elements for CO_2 chemiresistive sensing: electrical conductivity through a conjugated backbone, Lewis-basic N-heteroatoms, and protons for hydrogen-bond stabilization of charge-separated species. Its small nanopores (idealized 0.8 nm diameter) could further provide a good balance between accessibility to CO_2 binding sites and confined inclusion effects that combine to strongly enhance sensor−analyte interactions.[14] Notably, among all known conducting 2D MOFs, Cu_3HIB_2 is built from the smallest possible organic building unit and therefore exhibits the highest density of NH moieties.

Similar to amine-rich polymers, reversible formation of CO_2 adducts or bicarbonate salts can be conceived within Cu_3HIB_2 when the material is exposed to ambient conditions. CO_2 engaging in electron withdrawing interactions with amines, amounting to charge trapping with respect to the material, could give rise to direct chemiresistive modulation, as the amines are an integral part of the material's conjugated backbone (Figure 1c). To explore the potential for CO_2 sensing, we first explored the water and CO_2 adsorption properties of bulk Cu_3HIB_2. In contrast with nonporous amine-rich polymers, guest-accessible channels are intrinsic to the nanoporous structure of the MOF, and they remain accessible even after repeated thermal activation and prolonged exposure to dry or ambient conditions (Figures S1). Revealingly, the experimental H_2O adsorption isotherm for Cu_3HIB_2 showed distinct monolayer uptake in the range from zero to 5−10% RH (Figures 1d and S2). Fitting the H_2O sorption data to the Langmuir isotherm revealed monolayer coverage in the 0−20% RH range corresponding to 8.1 wt % H_2O uptake. This is consistent with filling of the sub-nanometer pores (approximately three H_2O molecules for each intrinsic cavity). By contrast, the much more gradual H_2O uptake at higher RH is indicative of structure-extrinsic, multilayer adsorption on grain boundaries and other structural defects. Importantly, the data reveal that the intrinsic hydration level of the MOF, corresponding to water uptake within the pores, should remain unchanged at values of RH greater than approximately 10% regardless of macroscopic sample morphology. The heat of adsorption for H_2O above 10% RH is relatively small, approximately 35−45 kJ mol^{-1}, and indicates reversible physisorption as the key interaction mechanism. Because the heat of adsorption of CO_2 itself is within the same range at low relative pressure of CO_2 (approximately 35−40 kJ mol^{-1}; Figures 1e and S3), exchange of H_2O with CO_2 should occur without a significant energy penalty. Whereas the heat of adsorption values are small for water, as its spontaneous condensation on surfaces under these conditions of pressure and temperature is anticipated, the equivalent range is quite large for noncondensable CO_2 but consistent with the formation of acid−base adducts between CO_2 and the N-heteroatoms in the pores of the 2D MOF.[34] Moreover, single-component isotherms often give lower-limit estimates of the

DOI: 10.1021/acscentsci.9b00482
ACS Cent. Sci. 2019, 5, 1425−1431

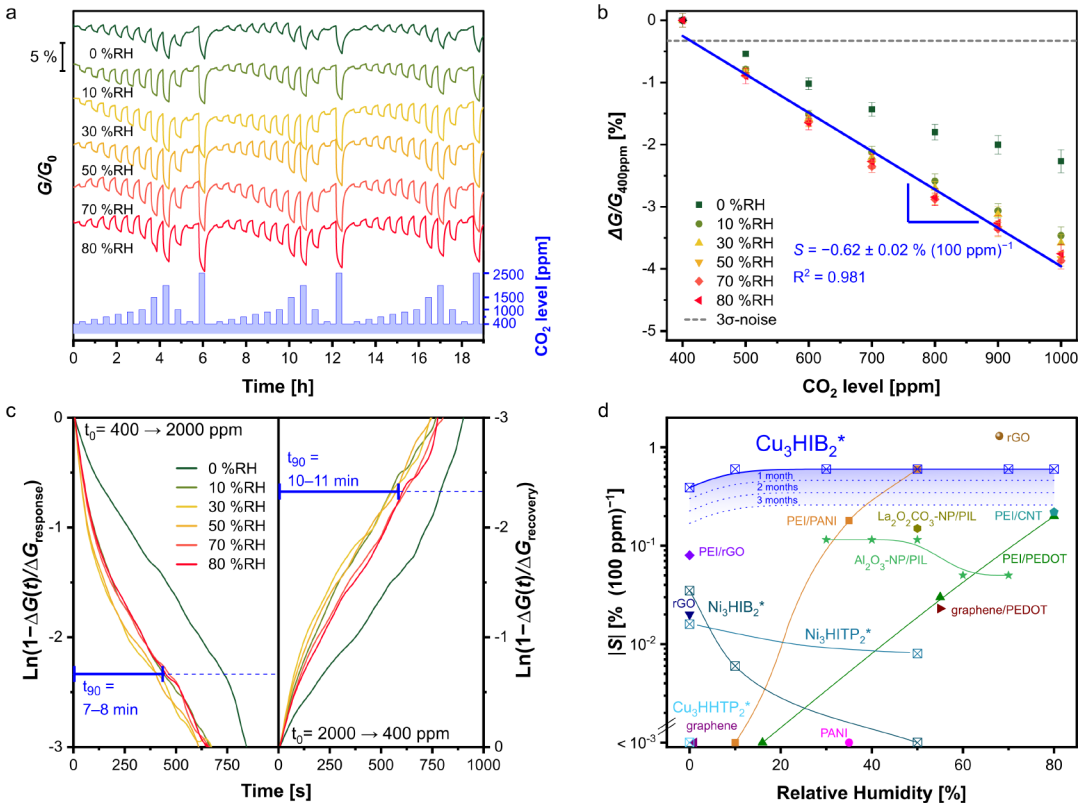

Figure 2. CO_2 chemiresistive sensing properties of Cu_3HIB_2 at room temperature in simulated humid air: (a) Normalized current−time traces (vertically offset for clarity) for one device measured consecutively at various variations of the CO_2 level respective to the 400 ppm baseline and at various constant RH values; (b) quantified responses between 400 and 1000 ppm (average and 1 standard deviation of mean response of 10 devices; blue line: linear fit of points acquired in the 10−80% RH range); (c) normalized response−recovery curves after an instant CO_2 level increase from 400 to 2000 ppm, and the corresponding decrease from 2000 to 400 ppm (each curve represents the noise-filtered average of 10 devices); (d) overview of the 500−1000 ppm of CO_2 sensing characteristics of solid-state chemiresistors reported in the literature and of the 2D MOFs tested as part of this work (indicated by asterisks). The evolution of the performance of Cu_3HIB_2 over a period of three months is indicated by the dotted lines. References: PANI, PEI/PANI;[16] PEI/PEDOT;[19] PEI/CNT;[18] rGO;[37,38] PEI/rGO;[39] graphene;[40] graphene/PEDOT;[41] $La_2O_2CO_3$−NP/PIL;[42] Al_2O_3−NP/PIL.[43]

ambient interactions, as markedly stronger interaction pathways can be anticipated for CO_2 and hydrated Cu_3HIB_2 (cf. bicarbonate formation, Figure 1c).

Chemiresistors were fabricated on interdigitated electrodes, by simply drop-casting as-synthesized suspensions of Cu_3HIB_2 as inks. The devices were loaded into a custom-built gas sensing cell (see experimental description) and conditioned for several hours under constant electrical bias and simulated ambient conditions. The CO_2 sensing performance of the devices was tested through direct-current amperometric (I−t) measurements at room temperature. The devices were subjected to different levels of CO_2 in the 400−2500 ppm range, i.e., from outdoors atmospheric level to the upper limit typically found indoors, in both increasing and decreasing CO_2 concentration regimes.[35] Each measurement was conducted at various levels of humidity in the range 0−80% RH, and 10 individual devices were tested over a total period of approximately 1 week. The normalized I−t traces, G/G_0, recorded for one of the 10 devices, are shown in Figure 2a (G_0 = initial baseline current). These experiments evidenced a clear "turn-off" response, i.e., inverse proportionality of the device conductance with the CO_2 level, and demonstrated highly repeatable and robust operation over 7 days of continuous experimentation.

The normalized responses between 400 and 1000 ppm, $\Delta G/G_{400\ ppm}$, are plotted as a function of CO_2 dosage in Figure 2b (see also Figure S4; $G_{400\ ppm}$ = current after recovery from each respective incremental dose). Notably, over the broad range of ambient conditions (10−80% RH), the response of the Cu_3HIB_2-based sensors is linear with respect to the CO_2 level and essentially RH-independent. The interpolated sensitivity (S) is −0.62% (100 ppm of CO_2)$^{-1}$, and the attainable signal resolution for a noise level of 3σ is 67 ppm. Despite the rather rudimentary nature of the drop-casted Cu_3HIB_2 sensors, their signal resolution is competitive with that of some commercial NDIR CO_2 sensors.[7] Intriguingly, these results also highlight the critical role of moisture in the performance of the devices: at humidity levels below 10% RH or under dry conditions, the sensitivity drops considerably. Such conditions are only found, however, during the driest days in the driest deserts, at very high altitudes, or in Antarctica.[36]

In Figure 2c, time-resolved analysis of the normalized response-recovery curves shows that the transient sensor characteristics reasonably obey first-order rate laws (i.e., approaching straight lines in the transformed semi-ln plot). The response and recovery times required to reach 90% of the saturation values (t_{90}) were in the range of 7−11 min for a shift between 400 and 2000 ppm and constant RH values between

DOI: 10.1021/acscentsci.9b00482
ACS Cent. Sci. 2019, 5, 1425−1431

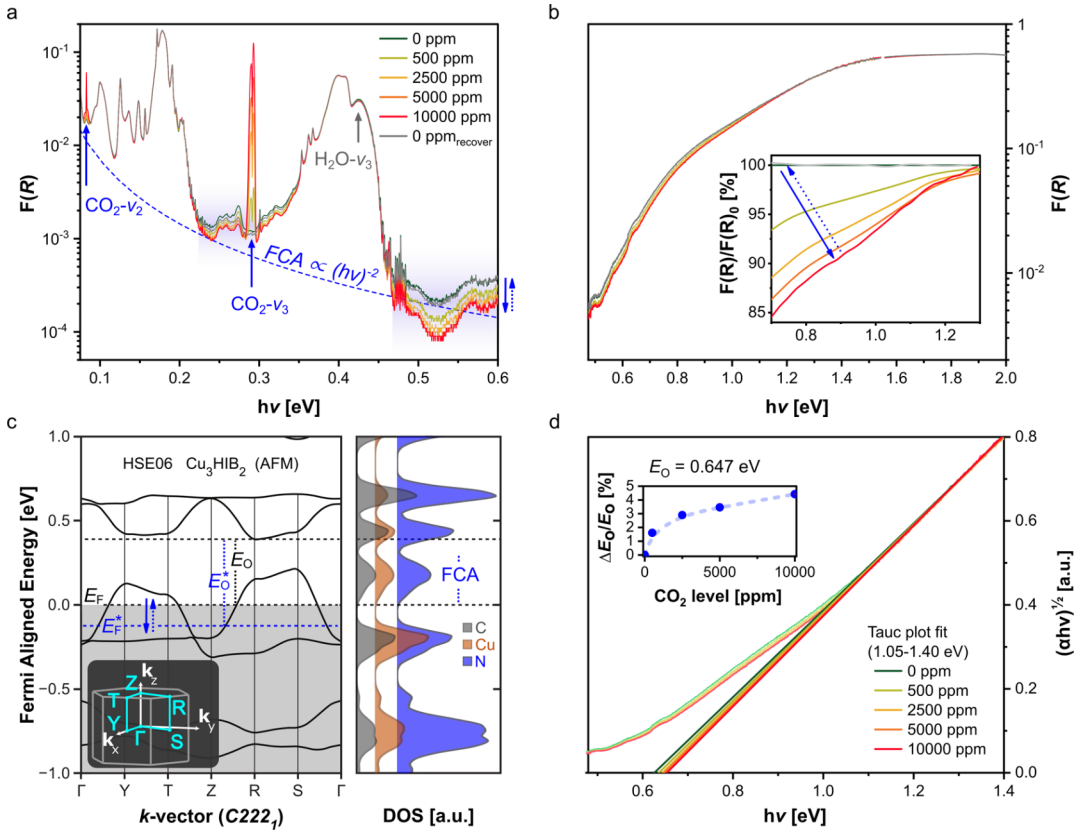

Figure 3. In situ spectroscopic probing of the electronic response of Cu_3HIB_2 under air at 50%RH. (a) Kubelka–Munk-transformed DRIFTS. The absorbance contributions that are not directly related to the organic vibrational modes of the material are labeled by arrows. The blue dashed line is the assignment of the contribution of free carrier absorbance (FCA). The blue double arrows indicate the background shift induced by adsorption (full line) and desorption (dotted line) of CO_2, respectively; (b) Kubelka–Munk-transformed NIR-DRS for the same color legend as panel a. The inset shows the shift in absorbance relative to the spectrum measured at 0 ppm of CO_2; (c) computed band structure of bulk $Cu_3(HIB)_2$. The expected widening of the optical band gap (E_O) upon decrease of the Fermi level is schematically illustrated (exaggerated for clarity). The inset shows the high-symmetry *K*-points of the first Brillouin zone; (d) Tauc plot fits of the data indicate Moss-Burstein widening of the band gap upon adsorption of CO_2 in humid Cu_3HIB_2. The inset shows the change of the fitted band gap energy relative to the spectrum at 0 ppm.

10 and 80%. Hence, the time resolution of the sensors is suitable for practical applications that require multiple measurements per hour. Consistent with the steady-state characteristics of the sensors, the normalized transient signals are nearly equivalent for the multiple simulated conditions of ambient RH. By contrast, the normalized kinetics were noticeably slower under simulated dry conditions (t_{90} = 12–13 min at 0% RH, dark green trace in Figure 2c). It should be noted, however, that even traces of water, which would be strongly adsorbed below 10% RH, are likely to promote CO_2 interactions under these conditions.

Figure 2d highlights the versatility of Cu_3HIB_2 as a CO_2 sensor relative to other materials reported for this application. In the relatively narrow, but expanding field of MOF-based sensors (see Table S1), Cu_3HIB_2 is the only material capable of detecting practically relevant CO_2 levels regardless of the transduction mechanism. More relevantly, the sensitivity of Cu_3HIB_2 is consistently the highest across the widest RH range reported thus far, even when compared to more complex sensor designs, e.g., meticulously downsized materials such as carbon nanotubes or few-layer graphene/graphene-oxide flakes and composite materials (see Table S2 for a detailed description of the entries in Figure 2d).

Even though long-term operation data beyond the range of a few days is seldom available for previous ambient CO_2 chemiresistors (see Table S2), the long-term stability of the Cu_3HIB_2 sensors—beyond the robust first week of operation shown in Figure 2a—was probed by repeating the test sequence at 50% RH on the same set of devices every 2 weeks for 3.5 months (Figure S5, dotted lines in Figure 2d). During this time, the sensitivity drifted, as is often observed with other chemiresistors.[44] Despite this gradual drop in absolute sensitivity, the signals remained fully analytical and predictable, and the sensitivity after three months under simulated real-world conditions was still RH-independent (Figure S6).

The remarkable performance of Cu_3HIB_2 as a CO_2 sensor and several data in Figure 2, most obviously the divergent behavior under dry conditions, point to a unique CO_2 capture/sensing mechanism that warrants further investigation. Indeed, the response of the Cu_3HIB_2 sensors at CO_2 levels below the atmospheric range (i.e., 0–500 ppm) is both stronger, S = −3.4% (100 ppm)$^{-1}$ and slower, t_{90} > 2 h (Figure S7). This is expected because the strongest adsorption sites are occupied by the first few molecules at a low CO_2 level. Although for Cu_3HIB_2 these strong adsorption sites do not influence the sensitivity in the relevant range of CO_2 concentration (i.e., above 400 ppm), these results show that tuning material properties to enhance sensitivity would likely come at the expense of response time.

DOI: 10.1021/acscentsci.9b00482
ACS Cent. Sci. 2019, 5, 1425–1431

To test the efficacy of related 2D conducting MOFs for CO_2 sensing, we investigated isomorphic materials made either from other transition metals or from differently functionalized organic ligands. Whereas all of these materials exhibited humidity responses similar to that of Cu_3HIB_2, roughly 0.2−0.5% (% RH)$^{-1}$ (Figure S8), none exhibited CO_2 sensitivity approaching that of the latter (Figure 2d, and Figures S9−11). Thus, Cu_3HOTP_2 (HOTP = 2,3,6,7,10,11-hexaoxytriphenylene), wherein copper nodes bridge semiquinonate (O) rather than imino-semiquinonate (NH) ligands, showed no measurable response at any CO_2 level. This confirms the important role of the imines in promoting interactions with CO_2 in Cu_3HIB_2. Ni_3HIB_2, the isostructural Ni analogue of Cu_3HIB_2, displayed "turn-on" responses, i.e., conductivity changes that were opposite in sign to those observed for the Cu analogue, that were nevertheless relatively small and were further negatively affected by increasing RH. Ni_3HITP_2 (HITP = 2,3,6,7,10,11-hexaiminosemiquinonatotriphenylene), an imine-containing MOF with a wider pore size, showed similar weak sensing characteristics. Notably, all imine materials exhibit a similar CO_2 uptake at low CO_2 pressure (Figure S12), suggesting that the vastly superior sensitivity of Cu_3HIB_2 relative to Ni_3HIB_2 and Ni_3HITP_2 is intrinsic and is likely related to electronic effects, as also addressed below.

Clues to the mechanism of CO_2 sensing in Cu_3HIB_2 came from investigating powder samples exposed to various levels of CO_2 at 50% RH by in situ diffuse-reflectance infrared Fourier-transform spectroscopy (DRIFTS) (Figure 3a). These spectra revealed important information about material stability as well as the first indications of electronic modulation of the MOF in the presence of CO_2. Thus, the vibrational modes pertaining to the organic ligands and the MOF lattice remained invariable at any level of CO_2 exposure, underlining the chemical stability of Cu_3HIB_2 under humid CO_2 atmosphere. Similarly, the frequencies of the characteristic ν_2 and ν_3 modes of CO_2 were nearly indistinguishable from those of gaseous CO_2, with only their intensities varying consistent with adsorptive accumulation (Figure S13). No characteristic modes for bicarbonate or carbamates were observed at CO_2 concentrations between 0−2500 ppm; these modes became apparent only weakly and only upon significantly raising the CO_2 level to 1−10% (i.e., 10 000−100 000 ppm; Figure S14). Analogous to the speciation of dissolved CO_2 in aqueous amine media,[45] the bicarbonate and carbamate salt fractions in Cu_3HIB_2 are presumed to be exceedingly small, particularly at typical ambient CO_2 levels. Most revealingly, increasing CO_2 levels cause a gradual decrease of the background IR absorbance of the material, most evident in the spectral ranges that are not dominated by strong vibrational modes from the MOF itself (e.g., hν = 0.5−0.6 eV and 0.25−0.3 eV). In degenerate or narrow-gap semiconductors, the background IR absorbance is generally associated with intraband excitation of free carriers in partially filled bands, also known as free carrier absorption (FCA).[46] FCA evolves inversely proportional with the square of the photon energy. Here, the decrease of background IR intensity with increasing CO_2 level is in line with a decrease of the free carrier concentration in Cu_3HIB_2.

The modulation of the free carrier concentration in Cu_3HIB_2 by CO_2 is corroborated by diffuse reflectance data in the near-infrared region. As shown in Figure 3b, the diminished background absorbance induced by CO_2 persists above the IR range up to approximately 1.2 eV, in agreement with the DRIFTS data. Qualitatively, the same data can be interpreted as a blue shift of the optical absorption edge, i.e., a widening of the optical band gap (Figure 3b, inset).

The computed band structure of Cu_3HIB_2, reported in previous work for the ideal crystal lattice devoid of included guest molecules,[32] shows a forbidden zone between the valence band and the conduction band (E_0, Figure 3c) and an indirect optical band gap. The position of the *Fermi level*, E_F, within the valence band, rather than the forbidden gap, as is typical for degenerately doped semiconductors, governs the photon energy required for the interband transition, i.e., the optical band gap (cf. *Moss−Burstein* shift).[47,48] As such, the band structure of Cu_3HIB_2 predicts a correlation between the indirect optical band gap and the Fermi level of the material: down shifting of E_F (denoted E_F* in Figure 3c) leads to widening of the optical band gap (E_0*).

The above treatment is in good agreement with the experimental NIR data transformed in Tauc coordinates for indirect interband transitions, $(\alpha h\nu)^{0.5}$, assuming proportionality between $F(R)$ and α, the absorption coefficient. This assumption can be made through dilution of the sample in an appropriate matrix. The linearized range of the Tauc plots—near the midpoint between the low and high absorbance ranges—was fitted and extrapolated to the intersection with the $h\nu$-axis (Figure 3d).[47,49,50] Through the shifting intersect, a clear widening of the optical gap, $\Delta E_0/E_0$ = +2−5% or 13−32 meV, is observed for exposure to 500−2500 ppm of CO_2. Notably, the incremental widening of the gap shows distinct saturation toward higher levels, consistent with the shape of the CO_2 adsorption isotherm and with the chemiresistive characteristics of the material (Figure 3d). Notably, similar absorbance background/band edge shifts are observable at different CO_2/H_2O ratios, consistent with the selective response to CO_2 under hydrated conditions (Figures S15). Importantly, although these data do not provide a molecular-level understanding of a particular CO_2 binding mode to Cu_3HIB_2, they are consistent with the hypothesis of charge trapping as a mechanism for CO_2 sensing, as proposed earlier. Indeed, water also induces background changes to the optical absorption data, but only below 10%RH, which we correlate with intrinsic water sorption. Above 10% RH, no significant further background modulation is observed (Figure S16), which is consistent with the water adsorption isotherm indicating extrinsic adsorption at RH > 10%. Notably, the low absorbance spectral region between the FCA and the onset of the absorption edge is not observed for Ni_3HIB_2 (Figure S17). The absence of this optical signature confirms the different electronic origin of the much weaker "turn-on" response of this 2D MOF.

In conclusion, conducting MOFs based on imino-semiquinonate moieties provide a powerful platform for chemiresistive sensing of ambient CO_2. Autogenous hydration of nanopores under ambient conditions provides remarkable independence of the CO_2 sensitivity with relative humidity, which contrasts strongly with previously reported CO_2 chemiresistors. Supported by electrical and spectroscopic data, we showed that compositional tuning of the 2D MOFs greatly impacts the CO_2 sensitivity. Encouraged by the robustness of our proof-of-concept sensors throughout months of use, and by the modularity and flexibility of the conducting 2D MOFs platform, these results provide a blueprint for tuning and optimizing chemiresistive responses for other host−guest pairs of interest.

DOI: 10.1021/acscentsci.9b00482
ACS Cent. Sci. 2019, 5, 1425−1431

METHODS

Device Preparation. Interdigitated electrodes (Pt, 200 μm line width; 150 μm interspacing) on ceramic supports were obtained from BVT Technologies (product ID: CC1.W2). All 2D MOFs samples were prepared according to slightly modified published procedures, as described in the Supporting Information. No unexpected or unusually high safety hazards were encountered. Colloidal inks (3 mg mL^{-1} in methanol) were prepared by ultrasonication using the freshly prepared, nondried 2D MOF powders. The inks were manually drop-casted on the active area of the substrate, by 1−2 μL amounts, at 45 °C using a hot plate and until the device resistances roughly stopped decreasing (typically, 5−10 droplets). The devices were baked for 15 min at 45 °C and stored under ambient conditions in closed gel-packs.

Gas Sensor Characterization. The gas sensor characterization was conducted at room temperature for up to 10 parallel devices using a home-built system consisting of a polytetrafluoroethylene cell and three Alicat mass-flow controllers. The Alicat Flow Vision software was used for programmed mixing of Airgas Ultra Zero synthetic air, synthetic air humidified using a scrubber filled with deionized water, and Airgas Research grade Carbon dioxide. A constant flow of 1 standard liter per minute (SLPM) was provided at the inlet of the cell (volume approximately 25 mL), and a mineral oil trap was connected to the outlet. The DC bias of the sensors was 0.8 V, and the currents were recorded in PalmSens PSTrace using a Palmsens EMstat3 equipped with a MUX-16 multiplexer (data acquisition rate: 0.5 Hz). Data analysis was conducted using a script in OriginLab OriginPro. Prior to the measurements, the devices were exposed to repeated hourly cycles of 0−500−1000 ppm of CO_2 at 50 RH until the baseline current stabilized (approximately residual drift smaller than −1% h^{-1} during the first 2 days, and smaller than −0.2% h^{-1} during the following weeks).

Adsorption Isotherms. The water and CO_2 adsorption isotherms were collected for 2D MOF powder samples (approximately 35 mg dry weight, preactivated at 100 °C under dynamic vacuum) using a Micromeritics ASAP 2020 equipped with vapor dosing option and an isothermal circulation bath for temperature control. The isosteric enthalpies of adsorption were calculated through evaluation of the temperature dependence of the pressure at equal surface coverage, using the Clausius−Clapeyron equation and measurement of the isotherms at three temperatures (15, 20, 25 °C).

In Situ Spectroscopy. Diffuse reflectance experiments were performed on carefully grinded mixtures of approximately 0.5 wt % 2D MOF in potassium bromide. All spectra are plotted with respect to the KBr background and after Kubelka−Munk transformation.

ASSOCIATED CONTENT

Supporting Information

The Supporting Information is available free of charge on the ACS Publications website at DOI: 10.1021/acscentsci.9b00482.

General procedures and experimental methods, Figures S1−17, Tables S1−S2 (PDF)

AUTHOR INFORMATION

Corresponding Author

*E-mail: mdinca@gmail.com.

ORCID

Ivo Stassen: 0000-0003-3997-653X
Jin-Hu Dou: 0000-0002-6920-9051
Christopher Hendon: 0000-0002-7132-768X
Mircea Dincă: 0000-0002-1262-1264

Notes

The authors declare the following competing financial interest(s): The authors have filed a patent application containing some of the results herein.

ACKNOWLEDGMENTS

I.S. is grateful to the Belgian American Educational Foundation (BAEF) and Research Foundation − Flanders (FWO) for postdoctoral fellowships. The authors thank Analog Devices, Inc. (ADI) for financial support. Fundamental studies of 2D MOFs are supported by the Army Research Office (Grant No. W911NF-17-1-0174). This work used the Extreme Science and Engineering Discovery Environment (XSEDE), which is supported by National Science Foundation grant number ACI-1548562.

REFERENCES

(1) Comini, E.; Faglia, G.; Sberveglieri, G. *Solid State Gas Sensing*; Springer US: Boston, MA, 2009.

(2) Korotcenkov, G. *Handbook of Gas Sensor Materials: Properties, Advantages and Shortcomings for Applications Vol. 1: Conventional Approaches; Integrated Analytical Systems*; Springer New York: New York, NY, 2013.

(3) Ahmed, K.; Kurnitski, J.; Sormunen, P. Demand Controlled Ventilation Indoor Climate and Energy Performance in a High Performance Building with Air Flow Rate Controlled Chilled Beams. *Energy Build.* **2015**, *109*, 115−126.

(4) Gruber, M.; Trüschel, A.; Dalenbäck, J.-O. CO_2 Sensors for Occupancy Estimations: Potential in Building Automation Applications. *Energy Build.* **2014**, *84*, 548−556.

(5) Puligundla, P.; Jung, J.; Ko, S. Carbon Dioxide Sensors for Intelligent Food Packaging Applications. *Food Control* **2012**, *25* (1), 328−333.

(6) Lewis, A. C. The Changing Face of Urban Air Pollution. *Science* **2018**, *359* (6377), 744−745.

(7) Dinh, T.-V.; Choi, I.-Y.; Son, Y.-S.; Kim, J.-C. A Review on Non-Dispersive Infrared Gas Sensors: Improvement of Sensor Detection Limit and Interference Correction. *Sens. Actuators B Chem.* **2016**, *231*, 529−538.

(8) Joo, S.; Brown, R. B. Chemical Sensors with Integrated Electronics. *Chem. Rev.* **2008**, *108* (2), 638−651.

(9) Barsan, N.; Weimar, U. Understanding the Fundamental Principles of Metal Oxide Based Gas Sensors; the Example of CO Sensing with SnO $_2$ Sensors in the Presence of Humidity. *J. Phys.: Condens. Matter* **2003**, *15* (20), R813−R839.

(10) Swager, T. M. Sensor Technologies Empowered by Materials and Molecular Innovations. *Angew. Chem., Int. Ed.* **2018**, *57* (16), 4248−4257.

(11) Joshi, N.; Hayasaka, T.; Liu, Y.; Liu, H.; Oliveira, O. N.; Lin, L. A Review on Chemiresistive Room Temperature Gas Sensors Based on Metal Oxide Nanostructures, Graphene and 2D Transition Metal Dichalcogenides. *Microchim. Acta* **2018**, *185* (4), 213.

(12) Latif, U.; Dickert, F. Graphene Hybrid Materials in Gas Sensing Applications. *Sensors* **2015**, *15* (12), 30504−30524.

(13) Chen, Z.; Deng, S.; Wei, H.; Wang, B.; Huang, J.; Yu, G. Activated Carbons and Amine-Modified Materials for Carbon Dioxide Capture — a Review. *Front. Environ. Sci. Eng.* **2013**, *7* (3), 326−340.

DOI: 10.1021/acscentsci.9b00482
ACS Cent. Sci. 2019, 5, 1425−1431

(14) Murphy, L. J.; Robertson, K. N.; Kemp, R. A.; Tuononen, H. M.; Clyburne, J. A. C. Structurally Simple Complexes of CO_2. *Chem. Commun.* **2015**, *51* (19), 3942−3956.
(15) Doan, T. C. D.; Baggerman, J.; Ramaneti, R.; Tong, H. D.; Marcelis, A. T. M.; van Rijn, C. J. M. Carbon Dioxide Detection with Polyethylenimine Blended with Polyelectrolytes. *Sens. Actuators B Chem.* **2014**, *201*, 452−459.
(16) Srinives, S.; Sarkar, T.; Hernandez, R.; Mulchandani, A. A Miniature Chemiresistor Sensor for Carbon Dioxide. *Anal. Chim. Acta* **2015**, *874*, 54−58.
(17) Yoon, B.; Choi, S.-J.; Swager, T. M.; Walsh, G. F. Switchable Single-Walled Carbon Nanotube−Polymer Composites for CO_2 Sensing. *ACS Appl. Mater. Interfaces* **2018**, *10* (39), 33373−33379.
(18) Star, A.; Han, T.-R.; Joshi, V.; Gabriel, J.-C. P.; Grüner, G. Nanoelectronic Carbon Dioxide Sensors. *Adv. Mater.* **2004**, *16* (22), 2049−2052.
(19) Chiang, C.-J.; Tsai, K.-T.; Lee, Y.-H.; Lin, H.-W.; Yang, Y.-L.; Shih, C.-C.; Lin, C.-Y.; Jeng, H.-A.; Weng, Y.-H.; Cheng, Y.-Y.; et al. In Situ Fabrication of Conducting Polymer Composite Film as a Chemical Resistive CO_2 Gas Sensor. *Microelectron. Eng.* **2013**, *111*, 409−415.
(20) Sheberla, D.; Sun, L.; Blood-Forsythe, M. A.; Er, S.; Wade, C. R.; Brozek, C. K.; Aspuru-Guzik, A.; Dincă, M. High Electrical Conductivity in Ni3(2,3,6,7,10,11- Hexaiminotriphenylene)2, a Semiconducting Metal-Organic Graphene Analogue. *J. Am. Chem. Soc.* **2014**, *136* (25), 8859−8862.
(21) Ko, M.; Mendecki, L.; Mirica, K. A. Conductive Two-Dimensional Metal−organic Frameworks as Multifunctional Materials. *Chem. Commun.* **2018**, *54* (57), 7873−7891.
(22) Rubio-Giménez, V.; Galbiati, M.; Castells-Gil, J.; Almora-Barrios, N.; Navarro-Sánchez, J.; Escorcia-Ariza, G.; Mattera, M.; Arnold, T.; Rawle, J.; Tatay, S.; et al. Bottom-Up Fabrication of Semiconductive Metal-Organic Framework Ultrathin Films. *Adv. Mater.* **2018**, *30*, 1704291.
(23) Sun, L.; Campbell, M. G.; Dincă, M. Electrically Conductive Porous Metal-Organic Frameworks. *Angew. Chem., Int. Ed.* **2016**, *55* (11), 3566−3579.
(24) Stassen, I.; Burtch, N.; Talin, A.; Falcaro, P.; Allendorf, M.; Ameloot, R. An Updated Roadmap for the Integration of Metal−organic Frameworks with Electronic Devices and Chemical Sensors. *Chem. Soc. Rev.* **2017**, *46* (11), 3185−3241.
(25) Campbell, M. G.; Liu, S. F.; Swager, T. M.; Dincă, M. Chemiresistive Sensor Arrays from Conductive 2D Metal−Organic Frameworks. *J. Am. Chem. Soc.* **2015**, *137* (43), 13780−13783.
(26) Campbell, M. G.; Sheberla, D.; Liu, S. F.; Swager, T. M.; Dincă, M. Cu_3(Hexaiminotriphenylene)$_2$: An Electrically Conductive 2D Metal-Organic Framework for Chemiresistive Sensing. *Angew. Chem., Int. Ed.* **2015**, *54* (14), 4349−4352.
(27) Smith, M. K.; Jensen, K. E.; Pivak, P. A.; Mirica, K. A. Direct Self-Assembly of Conductive Nanorods of Metal−Organic Frameworks into Chemiresistive Devices on Shrinkable Polymer Films. *Chem. Mater.* **2016**, *28* (15), 5264−5268.
(28) Ko, M.; Aykanat, A.; Smith, M.; Mirica, K. A. Drawing Sensors with Ball-Milled Blends of Metal-Organic Frameworks and Graphite. *Sensors* **2017**, *17* (10), 2192.
(29) Yao, M.-S.; Lv, X.-J.; Fu, Z.-H.; Li, W.-H.; Deng, W.-H.; Wu, G.-D.; Xu, G. Layer-by-Layer Assembled Conductive Metal-Organic Framework Nanofilms for Room-Temperature Chemiresistive Sensing. *Angew. Chem., Int. Ed.* **2017**, *56* (52), 16510−16514.
(30) Rubio-Giménez, V.; Almora-Barrios, N.; Escorcia-Ariza, G.; Galbiati, M.; Sessolo, M.; Tatay, S.; Martí-Gastaldo, C. Origin of the Chemiresistive Response of Ultrathin Films of Conductive Metal-Organic Frameworks. *Angew. Chem., Int. Ed.* **2018**, *57* (46), 15086−15090.
(31) Lahiri, N.; Lotfizadeh, N.; Tsuchikawa, R.; Deshpande, V. V.; Louie, J. Hexaaminobenzene as a Building Block for a Family of 2D Coordination Polymers. *J. Am. Chem. Soc.* **2017**, *139* (1), 19−22.
(32) Dou, J.-H.; Sun, L.; Ge, Y.; Li, W.; Hendon, C. H.; Li, J.; Gul, S.; Yano, J.; Stach, E. A.; Dincă, M. Signature of Metallic Behavior in the Metal−Organic Frameworks M_3(Hexaiminobenzene)$_2$ (M = Ni, Cu). *J. Am. Chem. Soc.* **2017**, *139* (39), 13608−13611.
(33) Feng, D.; Lei, T.; Lukatskaya, M. R.; Park, J.; Huang, Z.; Lee, M.; Shaw, L.; Chen, S.; Yakovenko, A. A.; Kulkarni, A.; et al. Robust and Conductive Two-Dimensional Metal−organic Frameworks with Exceptionally High Volumetric and Areal Capacitance. *Nat. Energy* **2018**, *3* (1), 30−36.
(34) Sumida, K.; Rogow, D. L.; Mason, J. A.; McDonald, T. M.; Bloch, E. D.; Herm, Z. R.; Bae, T.-H.; Long, J. R. Carbon Dioxide Capture in Metal-Organic Frameworks. *Chem. Rev.* **2012**, *112* (2), 724−781.
(35) Jones, A. P. Indoor Air Quality and Health. *Atmos. Environ.* **1999**, *33* (28), 4535−4564.
(36) Kerber, F.; Querel, R. R.; Rondanelli, R.; Hanuschik, R.; van den Ancker, M.; Cuevas, O.; Smette, A.; Smoker, J.; Rose, T.; Czekala, H. An Episode of Extremely Low Precipitable Water Vapour over Paranal Observatory. *Mon. Not. R. Astron. Soc.* **2014**, *439* (1), 247−255.
(37) Zhou, Y.; Jiang, Y.; Xie, T.; Tai, H.; Xie, G. A Novel Sensing Mechanism for Resistive Gas Sensors Based on Layered Reduced Graphene Oxide Thin Films at Room Temperature. *Sens. Actuators B Chem.* **2014**, *203*, 135−142.
(38) Muhammad Hafiz, S.; Ritikos, R.; Whitcher, T. J.; Md. Razib, N.; Bien, D. C. S.; Chanlek, N.; Nakajima, H.; Saisopa, T.; Songsiriritthigul, P.; Huang, N. M.; Rahman, S. A. A Practical Carbon Dioxide Gas Sensor Using Room-Temperature Hydrogen Plasma Reduced Graphene Oxide. *Sens. Actuators B Chem.* **2014**, *193*, 692−700.
(39) Zhou, Y.; Jiang, Y.; Xie, G.; Wu, M.; Tai, H. Gas Sensors for CO_2 Detection Based on RGO−PEI Films at Room Temperature. *Chin. Sci. Bull.* **2014**, *59* (17), 1999−2005.
(40) Smith, A. D.; Elgammal, K.; Fan, X.; Lemme, M. C.; Delin, A.; Rasander, M.; Bergqvist, L.; Schroder, S.; Fischer, A. C.; Niklaus, F.; Ostling, M. Graphene-Based CO_2 Sensing and Its Cross-Sensitivity with Humidity. *RSC Adv.* **2017**, *7* (36), 22329−22339.
(41) Andò, B.; Baglio, S.; Di Pasquale, G.; Pollicino, A.; D'Agata, S.; Gugliuzzo, C.; Lombardo, C.; Re, G. An Inkjet Printed CO_2 Gas Sensor. *Procedia Eng.* **2015**, *120*, 628−631.
(42) Willa, C.; Yuan, J.; Niederberger, M.; Koziej, D. When Nanoparticles Meet Poly(Ionic Liquid)s: Chemoresistive CO_2 Sensing at Room Temperature. *Adv. Funct. Mater.* **2015**, *25* (17), 2537−2542.
(43) Willa, C.; Schmid, A.; Briand, D.; Yuan, J.; Koziej, D. Lightweight, Room-Temperature CO_2 Gas Sensor Based on Rare-Earth Metal-Free Composites—An Impedance Study. *ACS Appl. Mater. Interfaces* **2017**, *9* (30), 25553−25558.
(44) Schüler, M.; Sauerwald, T.; Schütze, A. A Novel Approach for Detecting HMDSO Poisoning of Metal Oxide Gas Sensors and Improving Their Stability by Temperature Cycled Operation. *J. Sens. Sens. Syst.* **2015**, *4* (2), 305−311.
(45) Matin, N. S.; Remias, J. E.; Neathery, J. K.; Liu, K. Facile Method for Determination of Amine Speciation in CO_2 Capture Solutions. *Ind. Eng. Chem. Res.* **2012**, *51* (19), 6613−6618.
(46) Amalric Popescu, D.; Herrmann, J.-M.; Ensuque, A.; Bozon-Verduraz, F. Nanosized Tin Dioxide: Spectroscopic (UV−Vis, NIR, EPR) and Electrical Conductivity Studies. *Phys. Chem. Chem. Phys.* **2001**, *3* (12), 2522−2530.
(47) Chu, J.; Sher, A. *Physics and Properties of Narrow Gap Semiconductors*; Microdevices; Springer: New York, 2008.
(48) Kudman, I.; Seidel, T. Absorption Edge in Degenerate *p* -Type GaAs. *J. Appl. Phys.* **1962**, *33* (3), 771−773.
(49) Nowak, M.; Kauch, B.; Szperlich, P. Determination of Energy Band Gap of Nanocrystalline SbSI Using Diffuse Reflectance Spectroscopy. *Rev. Sci. Instrum.* **2009**, *80* (4), 046107.
(50) Gibbs, Z. M.; LaLonde, A.; Snyder, G. J. Optical Band Gap and the Burstein−Moss Effect in Iodine Doped PbTe Using Diffuse Reflectance Infrared Fourier Transform Spectroscopy. *New J. Phys.* **2013**, *15* (7), 075020.

DOI: 10.1021/acscentsci.9b00482
ACS Cent. Sci. 2019, 5, 1425−1431